24th Australasian Fluid Mechanics Conference – AFMC2024
Canberra Australia
1-5 December 2024
Paper No: AFMC2024-061

Urban heat island mitigation by a modular parklet during a heat wave event in Sydney

Qingyun Wu, Yuhan Huang*, Peter Irga

Centre for Green Technology, School of Civil and Environmental Engineering, University of Technology Sydney, Ultimo NSW 2007, Australia
* Email: yuhan.huang@uts.edu.au

Abstract

The research presented here numerically investigated the impact of a modular parklet on the urban heat island (UHI) effect, during a heat wave event in Sydney, Australia. The computational domain was meshed based on an ideal symmetric street canyon with a simplified parklet geometry. The parklet was modelled as a porous media with appropriate resistance, porosity, energy, and turbulence equations. The simulation also utilized ANSYS Fluent's solar calculator and discrete ordinate radiation model to determine the distribution of radiative heat fluxes on surfaces. Field experiments were conducted to collect ambient air temperature and air temperature near the parklet, which were used to validate the model. The simulation results indicated that the air temperature on the parklet is lower by 0.4 °C, and the parklet can cool the surrounding air at pedestrian height of over 0.1 °C. The wind velocity magnitude is reduced near the parklet, while the average wind velocity at pedestrian height is slightly higher (0.075 m s^{-1}) than the canyon without the parklet.

1. Introduction

Rapid urbanization is a global trend, with 57% of the world's population now residing in urban areas (World Bank 2024). While urbanization promotes human welfare, it also brings great challenges to the sustainability of the environment. Among these challenges, the urban heat island (UHI) effect and extreme heat events are prominent manifestations of surface warming in urban environments. UHI effect describes the phenomenon where the urban temperature is significantly higher than that in surrounding non-urban areas (Oke 1982). Such rising temperatures can increase the cooling energy load of buildings (Lee & Jim 2018). Moreover, UHI poses significant health issues for residents, potentially increasing the risk of heat-related diseases such as heat stroke and cardiovascular diseases (Xi *et al*. 2023). It is estimated that 6,700 premature deaths in 93 European cities can be attributed to UHI effects during the summer of 2015 (Iungman *et al*. 2023).

The impact of green infrastructure, such as street trees, hedges, green roofs and vertical greenery, on mitigating UHI has been widely investigated through field experiments and numerical simulations. They mainly alter the urban thermal environment through four mechanisms, i.e. providing shading, facilitating evapotranspiration, altering surface albedo and facilitating multisensory interaction (Gunawardena *et al*. 2017). Their effectiveness varies depending on the type of green infrastructure and geographic factors. For example, Lee and Jim (2018) conducted field experiments, and found that extensive green roofs can reduce air temperatures by up to 6.21 °C during bright sunny days in Hong Kong's summer months, and a dense woodland canopy with a 10-cm deep substrate can effectively minimize heat exchange with indoor spaces. Gülten *et al*. (2016) reported that street trees could lower daily heat island potential values by 6.8 °C in June in Elâzığ, Turkey, using computational fluid dynamic (CFD) simulations.

Street parklets are a common approach for 'placemaking' that provides various benefits, such as aesthetic enhancement and liveability improvement (Stevens *et al*. 2024). However, despite their long history and frequent use in urban planning, their role in mitigating the UHI effect is rarely investigated. Therefore, this study aims to investigate the performance of a single modular, removable parklet in mitigating the UHI effect within a street canyon during heat waves using CFD simulations.

This paper is organized as follows. Section 2 details the CFD simulation methodology, including the computational domain and geometry settings, governing equations and turbulence model, tree aerodynamic and transpiration effects, and boundary conditions. Section 3 describes the grid sensitivity analysis and validates the model by comparing temperature data from field experiments and simulations. Section 4 presents and discusses the simulation results. Finally, Section 5 concludes the paper and suggests future perspectives.

2. Methodology

The studied site was the Auburn Centre, Western Sydney, Australia (-33.8498, 151.0317, +GMT11). Sydney has a humid subtropical climate, and summer in Sydney is generally warm to hot (McDonald 2008). The geometry model of the street canyon and parklet was created in ANSYS SpaceClaim. This study employs a full-scale 3D street canyon model, consisting of an isolated, ideal street canyon configuration. The model features two identical concrete buildings in an east-west orientation. Each building has dimensions of 20 (W) × 20 (H) × 100 (L) m^3, corresponding to the x, y, and z axials (Figure 1a). The dimensions of the computational domain are based on the H as follows: the axial distance between velocity inlet and the windward face of the upstream building is 5H, the transverse distances between the sidewalls of each building and the symmetric boundaries on both ends are 5H, the distances between building roofs and top boundaries are 5H, and the outlet boundary is 15H from the leeward faces of the downstream buildings (Figure 1a), according to the practical guideline for building simulation using CFD method by Tominaga *et al*. (2008). In terms of modelling the parklet site, it was represented as a cuboid-shaped porous medium base for the entire shrub area, with dimensions of 3.6 (W) × 0.5 (H) × 3.6 (L) m^3, 0.1 m above the ground, and a simplified tree model cuboid with dimensions of 1.2 (W) × 1.8 (H) × 1.2 (L) m^3 on top of it (Figure 1b), based on the actual site (Figure 1c). The coordinate origin (0 m, 0 m, 0 m) is set at the centre of the street surface. The centre of the parklet's bottom surface is located at (0 m, 0.1 m, 0 m). The relative size of the parklet is depicted in Figure 1d, which shows the front view along the z-direction. The simulations were conducted for steady weather conditions on a clear summer day (1st February 2024) with a high temperature of 32 °C.

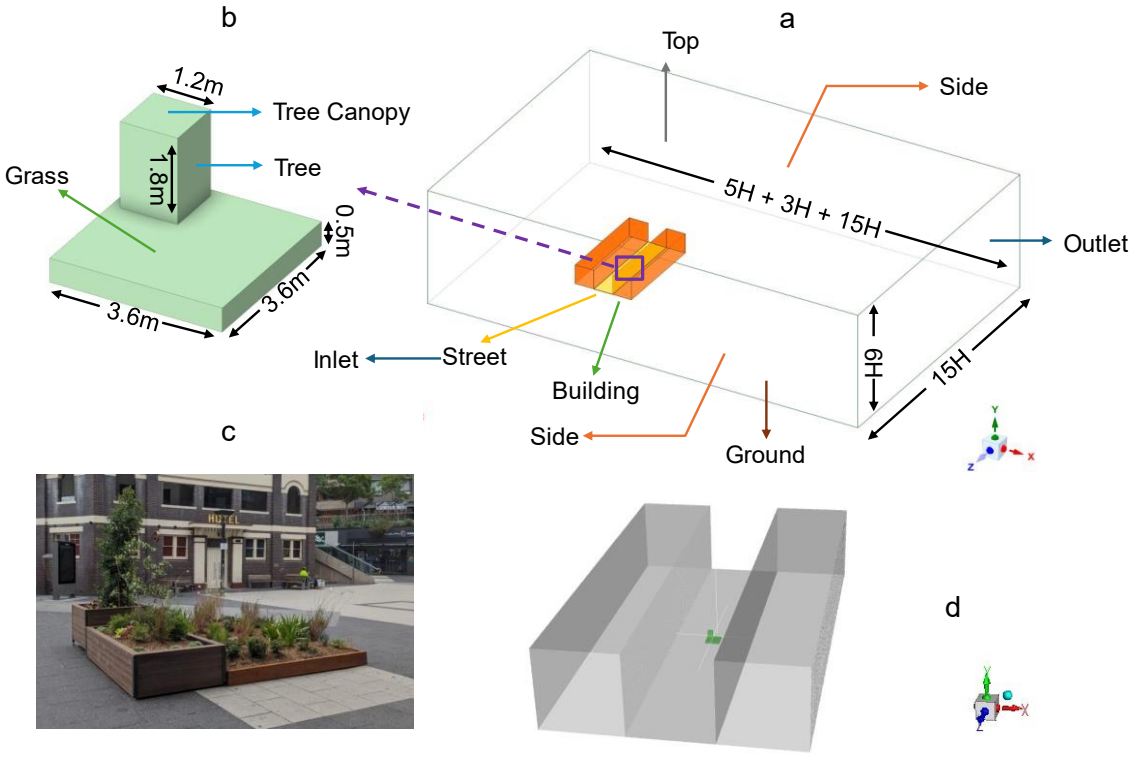

Figure 1. Building arrangement and dimensions of computational domain (a), parklet geometry (b), field experiment site of the parklet (c), relative size of the parklet compared to the street canyon and the location of reference lines (d).

The commercial CFD code ANSYS Fluent was employed to solve the steady-state 3D Reynolds-averaged Navier-Stokes equations with realizable $k-\varepsilon$ model, which has demonstrated better accuracy for building simulations, especially in terms of flow separation, recirculation, and flow involving rotation (Zhang *et al*. 2023). The SIMPLE numeric algorithm was adopted for pressure-velocity coupling, and the second-order upwind scheme was applied to discretize the convective and diffusion terms. The convergence criteria for the normalized residual errors of flow variables were set to 10^{-5}, and the mass balance check was set below 1%.

To calculate temperatures of buildings and ground surfaces, the Radiation-Solar Ray Tracing module was activated to provide accurate data on incident radiation. The Discrete Ordinates model was applied to calculate radiant heat fluxes between surfaces, using radiation intensity transport equations for gray diffuse walls. The built-in Solar Calculator was activated to account for the sun position. Simulations considered the shading of buildings while neglecting the shading effect of the parklet.

The parklet was treated as a porous medium to model the effects of vegetation on air flow. The approach that can explain the additional dissipation of turbulent kinetic energy caused by the turbulence cascade's spectral short-circuiting mechanism was adopted (Gromke *et al*. 2015, Gülten *et al*. 2016). This method can accurately predict the increased turbulent dissipation of air flows through plants. Source terms for the momentum equation (S_{u_i}), turbulent kinetic energy equation (S_k), and turbulent dissipation rate equation (S_ε) of the vegetation are set as follows:

$$S_{u_i} = -\rho C_d \mathrm{LAD} U_i \mathbf{U} \tag{1}$$

$$S_k = \rho C_d \mathrm{LAD}\left(\beta_p \mathbf{U}^3 - \beta_d \mathbf{U} k\right) \tag{2}$$

$$S_\varepsilon = \rho C_d \mathrm{LAD} \frac{\varepsilon}{k}\left(C_{\varepsilon 4}\beta_p \mathbf{U}^3 - C_{\varepsilon 5}\beta_d \mathbf{U} k\right) \tag{3}$$

where ρ is the air density, $C_d = 0.2$ represents the drag coefficient, LAD = 2 m^2 m^{-3} represents the average leaf area density of the shrub bottom and tree (Buccolieri *et al*. 2019), U_i represents the velocity component in the axial direction i, $\mathbf{U}$ represents the velocity magnitude, β_p represents the fraction of mean kinetic energy converted into turbulent kinetic energy, β_d represents the coefficient for the short-circuiting of the turbulence cascade, k represents the turbulent kinetic energy, ε represents the dissipation rate, and $C_{\varepsilon 4} = C_{\varepsilon 5} = 0.9$ are two model constants. The inertial resistance and porosity of plants were set as 9.5 m^{-1} and 0.4, respectively.

To model the transpirational cooling of plants, this study incorporated energy equation to represent the amount of thermal energy absorbed by the planter (S_T) (Gülten *et al*. 2016). The source term for the energy equation is expressed as:

$$S_T = R_{n,vol} - \mathrm{LAD}(LE_v + Q_{conv}) \tag{4}$$

where $R_{n,vol}$ represents the volumetric net radiation (W m^{-3}), and LE_v and Q_{conv} represent the latent heat (J kg^{-1}) and heat flux (W m^{-2}) of the plants, respectively.

Regarding the boundary conditions, a power-law velocity profile U was applied at the inlet, along with turbulent kinetic energy k, and turbulent dissipation rate ε in the atmospheric boundary layer (Li *et al*. 2023):

$$U(y) = U_{ref}\left(\frac{y}{y_{ref}}\right)^a \tag{5}$$

$$k(y) = (U(y) \times I_{in})^2 \tag{6}$$

$$\varepsilon\,(y) = \frac{C_\mu^{3/4} k(y)^{3/2}}{\kappa y} \tag{7}$$

where $y_{ref} = 20$ m represents the reference height, $a = 0.22$ represents the power-law exponent that stands for underlying surface roughness above the urban area, $I_{in} = 0.1$ represents the turbulent intensity, $\kappa = 0.42$ represents the von Karman's constant, $C_\mu = 0.085$ is the model constant, and $U_{ref} = 6$ m s^{-1} is the reference flow velocity.

Conduction equations were activated for all wall boundaries to capture heat transfer through these walls. The thermo-physical and spectral optical properties of these boundaries are detailed in Table 1. Building roofs were assigned different absorption coefficient and emissivity due to their lighter colour. The top and lateral boundaries of the computational domain were treated as symmetry boundaries. The heat transfer coefficients h_c of wall boundaries were calculated based on the empirical equations derived from wind tunnel measurements (Mirsadeghi *et al*. 2013):

For roofs:

$$h_c = 4.1V_R + 5.8 \tag{8}$$

For other surfaces:

$$h_c = 4.1(2/3\,V_R) + 5.8 \tag{9}$$

where $V_R = 3$ m s^{-1} for typical buildings with height between 4 and 8 stories in city centres, which corresponds to the conditions of this study. Standard wall functions were applied at the building and street surfaces. The surface roughness height K_s is calculated by aerodynamic roughness $z_0 = 2$ m and roughness constant $C_s = 0.5$ as follows:

$$K_s = \frac{9.793 z_0}{C_s} \tag{10}$$

Property	Fluid	Building & street surface	Building roof	Plant
Materials	Air	Concrete	Concrete	Porous materials
Density (kg m^{-3})	1.225	2391.7	2391.7	700
Specific heat (J kg^{-1} K^{-1})	1006.43	936.35	936.35	2310
Thermal conductivity (W m^{-1} K^{-1})	0.042	2.0712	2.0712	0.17
Viscosity (kg m^{-1} S^{-1})	1.7894×10^{-5}	-	-	-
Absorption coefficient (m^{-1})	0.19	0.6	0.4	0.46
Scattering coefficient (m^{-1})	0	0	0	0
Refractive index	1	1.7	1.7	2.77
Emissivity	0.9	0.7	0.8	0.46

Table 1. Thermo-physical and spectral optical properties of materials used (Gülten *et al*. 2016, Yang *et al*. 2017).

3. Grid sensitivity analysis and validation

Polyhedral cells were used to generate grids since this method balances accuracy and computational cost in wind field simulations around buildings (Wang *et al*. 2021). Coarse, medium, and fine meshes, consisting of 245,909, 620,114, 1,784,063 cells, respectively, were compared to identify the most suitable grid for calculation. At least 10 cells are meshed on side of the buildings with a stretching ratio of 1.2 (Tominaga *et al*. 2008). Figure 2 compares the air temperature and airflow velocity magnitude from three grid sets along the vertical line within the street canyon at a z-coordinate of -5 m. The location of this vertical reference line is shown in Figure 1d. As shown in Figure 2, the fine and medium grids provide similar results, while larger deviations are observed between the coarse grid and the other grid in terms of velocity magnitude. Consequently, the medium grid was considered adequate and computationally cost-efficient, and was used for the subsequent simulations. The rapid temperature change near height = 0 m is due to the proximity to the building walls whose surface temperature is significantly higher than the air temperature.

The simulations were validated against field experiment data collected at 9:00 and 14:00. One parklet site was placed at the centre of the street canyon. Temperature measurements were taken near

the junction of tree foliage and grass, as well as ambient air temperature 3 m away from the centre of the parklet toward the leeward wall direction at a pedestrian height of 1.5 m, using iButton temperature data loggers. As shown in Figure 3, the numerical and experimental results of air temperature agree well.

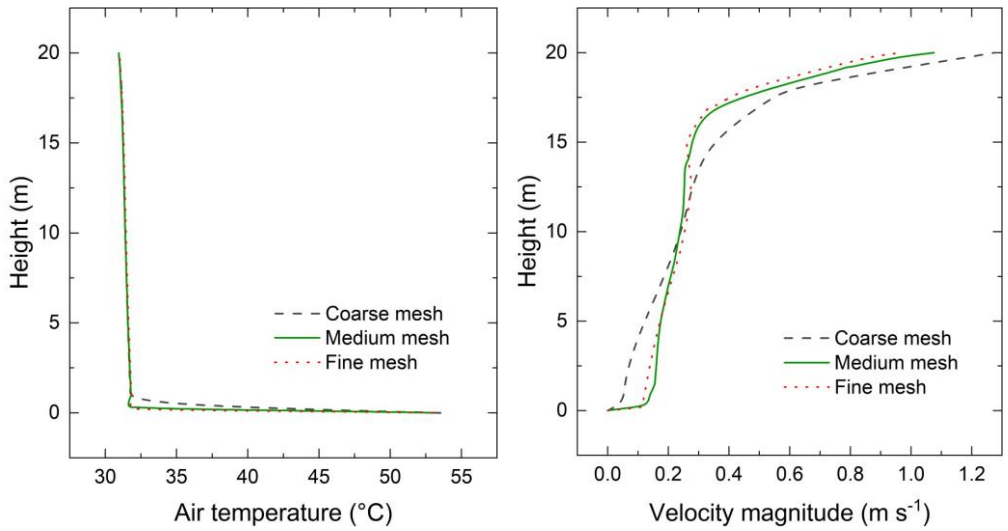

Figure 2. Comparison of the air temperature and velocity magnitude distributions along the vertical reference line inside the street canyon using different mesh densities.

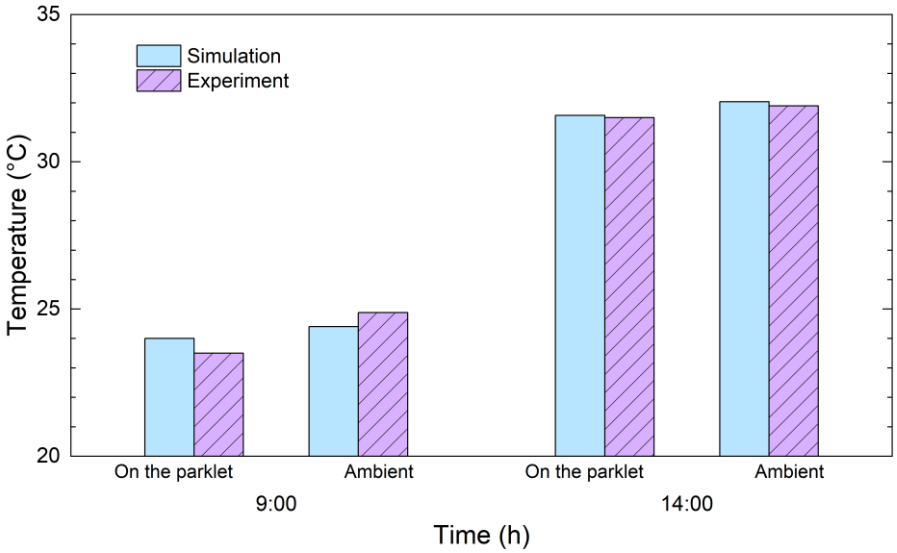

Figure 3. Comparison of simulated and experimental air temperatures at 9:00 and 14:00 for the parklet and ambient measurements.

4. Sample simulation results and discussion

The sample simulation scenario was conducted for 14:00 local time. Two lines along the x and z directions at pedestrian height were chosen to display the air temperature and velocity magnitude distribution (the location is shown in Figure 1d). The simulated and experimental air temperatures on the parklet are 0.46 °C and 0.40 °C lower than the ambient air temperatures at the measurement point (Figure 3). To illustrate the impact of the parklet, a scenario of the canyon without the parklet was compared against the simulation results. As shown in Figures 4a and 4c, the temperature decreases by over 0.1 °C around the parklet domain along both x and z lines, and this decrease extends further in both directions. This can be attributed to the transpiration effect of vegetation. However, direct solar radiation could significantly weaken the cooling performance of vegetation since the parklet is not shaded by any building. Across the entire plane at pedestrian height within the canyon, the air temperature is 0.04 °C lower than in the canyon without the parklet (Figure 5).

The airflow velocity in the central area of the canyon is lower than at both ends, with the magnitude decreasing as it approaches the building walls (Figures 4b and 4d). This reduction could be attributed to reduced air exchange with the environment outside the canyon, potentially leading to heat accumulation in the central area near the leeward wall and lower temperatures at both ends of the canyon (Figures 5a and 5b). The average airflow velocity magnitude at pedestrian height across the canyon is 0.075 m s^{-1} higher in scenario with the parklet, compared to scenario without. The airflow velocity magnitude decreases near the parklet along the x direction while increasing above the parklet base (Figure 4b), similar to findings in simulations by (Li *et al*. 2023). In addition, the airflow velocity decreases when approaching the parklet from the positive z direction as well, while it increases slightly around the central area of the parklet (Figure 4d).

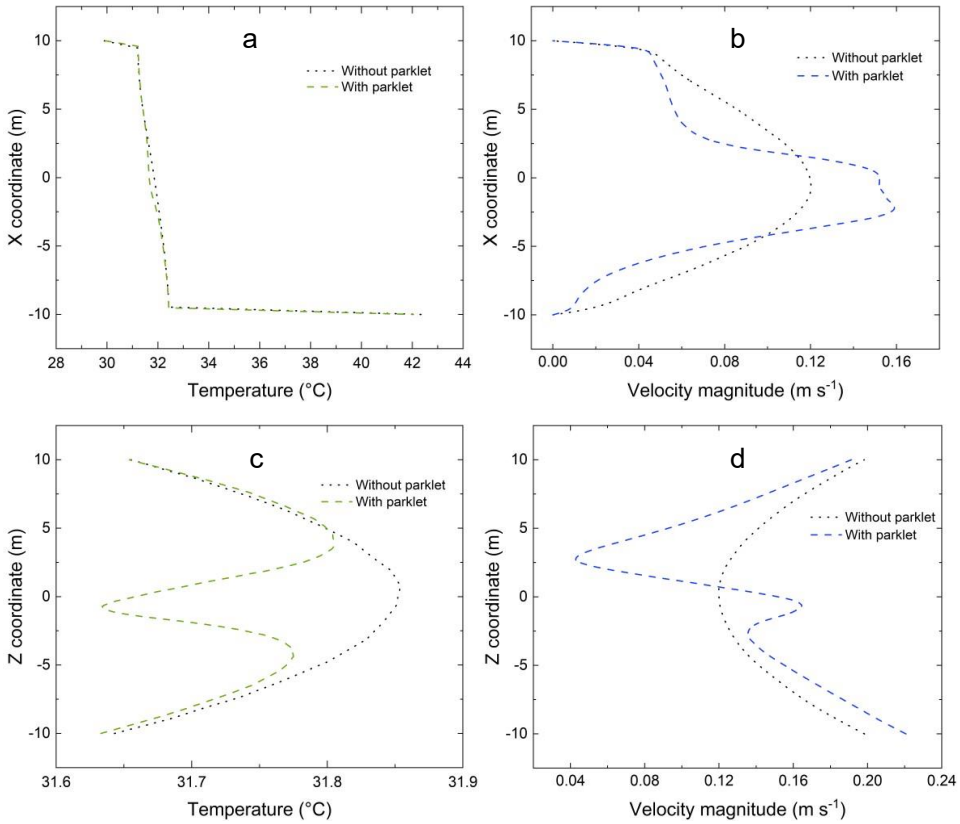

Figure 4. Comparison of simulated air temperature and velocity magnitude distributions at pedestrian height with and without the parklet at 14:00 local time. (a) Temperature along the x-coordinate. (b) Velocity magnitude along the x-coordinate. (c) Temperature along the z-coordinate. (d) Velocity magnitude along the z-coordinate.

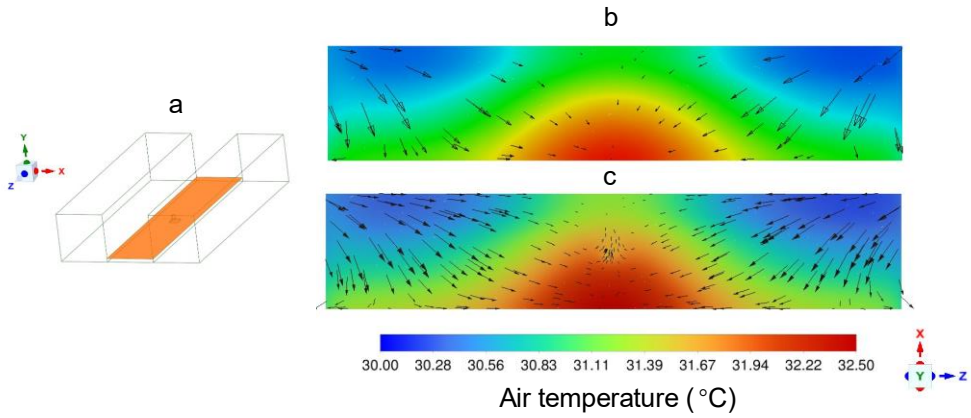

Figure 5. (a) Location of pedestrian-height plane. Top-down views of air temperature contours and airflow distribution of (b) scenario without the parklet and (c) scenario with the parklet.

5. Conclusion and future perspectives

A numerical model was developed to investigate the cooling effect of a modular parklet on the UHI effect. This model included the full-scale computational domain, featuring a symmetric street canyon, and the plant-based parklet consisting of porous media. The gird sensitivity test was conducted to select the grid balancing accuracy and computational cost. The model demonstrated minor deviations from experimental data, indicating its validity. Sample simulation results showed that a single mobile parklet could decrease the temperature of its vegetation and the surrounding environment, even without accounting for the shading effect. While these results are not as pronounced as those from other studies on street trees (e.g., 0.94 ℃ air temperature reduction in a meta-analysis of 24 studies on urban parks (Bowler *et al*. 2010)), this study shows the parklet's potential to further reduce heat stress for pedestrians, in addition to its aesthetic and liveability benefits.

The current research focused on a single parklet site. Further investigation can refine the parklet site model by detailing the soil composition, shrub cluster allocation, and the panel materials comprising the edgings and bottom of the parklet. Moreover, the study can be expanded to explore different wind flow conditions and varied urban cooling strategies, such as additional ground-level and rooftop installations of parklets, providing richer insights into sustainable urban design practices.

5. Acknowledgements

This project was supported by the Small Business Innovation & Research (SBIR) Program: The Office of the NSW Chief Scientist & Engineer (OCSE), and Future Village Placemaking Pty Ltd. Y.H. and P.I. are recipients of the ARC Discovery Early Career Research Award (DE220100552, DE210100755).

References

Bowler, D. E., Buyung-Ali, L., Knight, T. M., & Pullin, A. S. 2010, Urban greening to cool towns and cities: A systematic review of the empirical evidence, *Landsc. Urban Plan.*, **97**(3), 147–155.

Buccolieri, R., Santiago JL., Rivas, E., & Sáanchez, B. 2019, Reprint of: Review on urban tree modelling in CFD simulations: Aerodynamic, deposition and thermal effects, *Urban For. Urban Green.*, **37**, 56–64.

Gromke, C., Blocken, B., Janssen, W., Merema, B., van Hooff, T., & Timmermans, H. 2015, CFD analysis of transpirational cooling by vegetation: Case study for specific meteorological conditions during a heat wave in Arnhem, Netherlands, *Build. Environ.*, **83**, 11–26.

Gülten, A., Aksoy, U.T., & Öztop, H.F. 2016, Influence of trees on heat island potential in an urban canyon, *Sustain. Cities Soc.*, **26**, 407–418.

Gunawardena, K.R., Wells, M.J., & Kershaw, T. 2017, Utilising green and bluespace to mitigate urban heat island intensity, *Sci. Total Environ.*, **584–585**, 1040–1055.

Iungman, T., Cirach, M., Marando, F., Barboza, E.P., & Khomenko. S. 2023, Cooling cities through urban green infrastructure: a health impact assessment of European cities, *The Lancet*, **401**, no. 10376, 577–589.

Lee, L.S.H. & Jim, C.Y. 2018, Thermal-cooling performance of subtropical green roof with deep substrate and woodland vegetation, *Ecol. Eng.*, **119**, 8–18.

Li, Z., Zhang, H., Juan, Y.H., Lee, Y.T., Wen, C.Y., & Yang, A.S. 2023, Effects of urban tree planting on thermal comfort and air quality in the street canyon in a subtropical climate, *Sustain. Cities Soc.*, **91**, 104334.

McDonald, J. 2008, *Dreamtime Superhighway: Sydney Basin Rock Art and Prehistoric Information Exchange*, Australian National University E-Press, Canberra.

Mirsadeghi, M., Cóstola, D., Blocken, B., & Hensen J. L. M. 2013, Review of external convective heat transfer coefficient models in building energy simulation programs: Implementation and uncertainty, *Appl. Therm. Eng.*, **56**, no. 1–2, 134–151.

Oke, T.R. 1982, The energetic basis of the urban heat island, *Q. J. Roy.*, **108**, no. 455, 1–24.

Stevens, Q., Leorke, D., Thai, H. M. H., Innocent. T., & Tolentino, C. 2024, Playful, portable, pliable interventions into street spaces: deploying a “playful parklet” across Melbourne’s suburbs, *J. Urban Des.*, **29**, no. 2, 231–251.

Tominaga, Y., Mochida, A., Yoshie, R., Kataoka, H., Nozu, T., Yoshikawa, M., & Shirasawa, T. 2008, AIJ guidelines for practical applications of CFD to pedestrian wind environment around buildings, *J. Wind. Eng. Ind. Aerodyn.*, **96**, no. 10–11, 1749–1761.

Wang, W., Cao, Y., & Okaze, T. 2021, Comparison of hexahedral, tetrahedral and polyhedral cells for reproducing the wind field around an isolated building by LES, *Build. Environ.*, **195**, 107717.

World Bank 2024, *Urban Development*, *World Bank*, viewed 22 July 2024, <https://www.worldbank.org/en/topic/urbandevelopment>.

Xi, C., Han, L., Wang., J., Feng, Z., Kumar, P., & Cao, S. J. 2023, How can greenery space mitigate urban heat island? An analysis of cooling effect, carbon sequestration, and nurturing cost at the street scale, *J. Clean. Prod.*, **419**, 138230.

Yang, A.S., Juan, Y.H., Wen, C.Y., & Chang, C.J. 2017, Numerical simulation of cooling effect of vegetation enhancement in a subtropical urban park, *Appl. Energy*, **192**, 178–200.

Zhang, X., Buddhika, J.W.G., Wang, J., Weerasuriya, A.U., & Tse, K.T. 2023, Numerical investigation of effects of trees on cross-ventilation of an isolated building, *J. Build. Eng.*, **73**, 106808.